Development and Characterization of SDS Doped Poly(aniline-*co*-2-isopropylaniline) MWCNT/CuO Nanocomposites for Electrochemical Supercapacitor Application

Kamal Kant Singh and Ashok K. Sharma[*]

Film Laboratory, Department of Materials Science & Nanotechnology, Deenbandhu Chhotu Ram University of Science & Technology, Murthal-131039, India

*Corresponding author: E-mail: ashokksharma2k18@gmail.com

A novel electroactive nanocomposite material containing aniline-*co*-2-isopropylaniline (Pani-co), SDS doped poly-Pani-co, copper oxide (CuO), and multiwalled carbon nanotubes (MWCNTs) has been developed by *in situ* oxidative synthesis technique. The electrochemical execution of synthesised composite as electroactive supercapacitor material was examined through three electrode cell assembly *viz.* cyclic voltammetry (CV), galvanostatic charge/discharge analysis (GCD) and electrochemical impedance study. Physical and chemical characteristics of synthesized SDS doped Pani-co/MWCNT/CuO nanocomposite were explored *via* FTIR, TGA, XRD, FESEM and EDX methods. The results confirmed that the existence of metal oxide on MWCNTs enhanced the redox activity of the prepared composite. The maximum specific capacitance obtained in cyclic voltammetric studies was 1473 F/g at sweep rate of 3mV/s, and the maximum specific capacitance obtained with GCD studies was 1512 F/g at current density of 1A/g in 1M Na_2SO_4 aqueous solution of with better cycle life.

Keywords: 2-Isopropylaniline, Carbon nanotubes, Supercapacitor, Voltammetry, Charge-discharge, Copper oxide.

INTRODUCTION

Recently, electrochemical supercapacitors have allured many researchers interest being excellent energy storage systems. They are utilized as premier energy storage purpose or as fuel cells or batteries. They show appreciable power density that they can overcome the lack of reusable batteries in the energy conservation area. They are classified into two types of energy storage devices, on basis of mechanisms for supercapacitors capacitive charge storage; electric double layer (EDLC) and pseudocapacitive. The device characteristics based on pseudo-capacitance are superior to those of electric double layer capacitance. However, the phase change inside the pseudo-capacitance based devices curtails their lifespan and degrades the power density due to the effect of Faradic reaction. Several nanomaterials, carbonaceous materials, conducting polymers and transition metal oxides have been employed as supercapacitors electroactive materials. Carboneous materials, usually referring to electric double layer capacitance are the most appropriate materials for supercapacitors. The enhanced capacitance of carbonaceous materials is possible because of standardi-zation of porosity and surface processing which further leads stability [1-5]. Till now, many carbon based materials and transitions metal oxides have already been tested as electro-active materials for electrochemical supercapacitor. Apparently owing appreciable capacitance as a result of their high specific power levels, metal oxides have been broadly utilized in comm-ercial appliances. They also emerged as a class of selection for supercapacitor and sensing applications [6-11]. Metal oxides are taken as priority materials because they offer higher surface areas, super electrical conductivities, prolonged charge/discharge cycle life, higher capacitance and better mechanistic aspects [12,13]. In the group of metal oxide, copper oxide, having a less energy band gap (~1.2 eV) exhibit p-type semiconductor nature and it is ultimate suitable candidate for supercapacitor electoactive materials as it is eco-friendly and very cost effective. A number of investigate has been convey in the field of nanotechnology lead by MWCNT. It is well in trend to take advantage of this exclusive one-dimensional nanomaterials in various fields like energy accumulation apparatus, field-emi-ssion, molecular equipments, *etc*. Due to their special physio-chemical aspects, MW-CNTs were widely accepted as exce-

llent electroactive material for ultra high power energy storage devices owing to its specific hollow structure, super electrical conductivity and high specific surface area [15-17]. Chemically-treated MWCNTs facilitates easy dispersion in organic solvents as well as in water. As if now the chemical treatment of CNTs were achieved by various mechanisms, as with non-covalent inter linkage for example bending, layer-to-layer, self-build, surface coating technique, cross-linkage with electrochemical coating on CNTs [18-20].

At present, there are various studies that directly involve MW-CNTs as an electroactive material. Many researchers have indicated that the pseudo capacitive capacitance of a capacitor work on Faradic redox reaction provide better capacity compare to the ELDC. Normally, thin film coating of materials which have redox action, for example metal oxide otherwise conductive polymer on the surface of MWCNTs are consider to raise the capacitance [21]. It has been concluded that the physico-chemical characteristics (mechanical, temperature stability, electrical conductivity and redox aspects) of polyaniline can be markedly enhanced by doping with sodium dodecylsulfate (SDS) [22,23]. SDS induces the surfactant molecules into the polymer thus altering the structural and electrochemical properties of the substrate [24,25]. Further, SDS is an excellent dispersing agent effectively applied for the stabilization of MWCNTs and nanoparticles [26-28]. Consequently, mixing of SDS gives electrochemical deposition of polyaniline in carbon particles suspensions and thus formation of electro-active composite thin film. Composite of polyaniline based electroactive materials on carbon nanoparticles or MWCNTs are of great efficiency for commercial application as energy storage devices, detector and fuel cells materials [29,30].

In the present study, a fabrication of proficient SDS doped poly-Pani-co/MWCNTs/CuO nanocomposite through *in situ* technique is reported. The composites comprising SDS doped Pani-co coated over CuO-doped MWCNTs were fabricated as advanced electroactive composite used for energy storage application as it providing unique morphology and excellent electro-capacitive performance.

EXPERIMENTAL

Aniline (99%, Merck) and copolymer 2-isopropylaniline (95% Merck) were purified in the vacuum prior to utilization. MWCNTs has external width 10-12 nm with extent 1-1 µm was purchased through Sigma-Aldrich, Acetylene black and poly-vinylidene fluoride (PVDF) was too acquire from Sigma-Aldrich. Other reagents like ammonium persulfate (APS), hydrochloric acid, sulphuric acid, nitric acid, ethanol and *N,N*-dimethyl forma-mide (DMF) were obtained from Himedia and utilized as acquired. Double distilled water (DDW) was used for all the synthesis.

Synthesis: step-1: First of all, MWCNTs functionalization was achieved by chemical acidified methods. Around 0.5 g of MWCNTs soaked in mixture of conc. H_2SO_4 and HNO_3 in the ratio of 1:3(v/v) for 10 h at room temperature. After this, above mixture was ultra-sonicated for 3 h. Afterward the functionalized MWCNTs were filtered through Whatman-1 filter paper (125 mm porosity). The functionalized MWCNTs washed through

with double distilled water up to neutralized pH of MWCNTs and then dried 100 ± 5 ºC for 5 h.

Step-2: The synthesis procedure for the preparation of SDS doped copolymers of aniline with poly(2-iso-propylaniline) (Pani-co) is as follows: A 0.326 g (0.01 mol) of SDS was added in 50 mL of distilled water. Then 0.05 mol (0.466 g) of aniline and 0.05 mol (0.685 g) of 2-iso-propylaniline were added into the SDS solution along with 10 mL (1 mol) HCl. Then 0.1 mol (2.28 g) of ammonium persulfate solution was mixed dropwise into the mixture. The reaction mixture was mechani-cally stirred for 24 h. The polymerization reaction temperature of the above solution was maintained in between 0 to 5 ºC. A green coloured precipitate was obtained. The obtained preci-pitate was washed with double distilled water and acetone to remove the unreacted monomers and oligomers. Obtained preci-pitates were dried using a vacuum oven at 90 ºC for 12 h and then characterized by different techniques. Similar procedure was followed to obtain copolymer with equal (1:1) ratio bet-ween aniline and 2-isopropylaniline with MWCNTs sample and copper oxide and these composite samples were denoted as SD1, SD2 and SD3, respectively (Table-1).

TABLE-1 COMPOSITION OF SAMPLE				
Sample	Aniline	Co-polymer	CNTs	Metal oxide (CuO)
SD1	0.05 M	0.05 M	0.05 g	–
SD2	0.05 M	0.05 M	–	0.2 g
SD3	0.05 M	0.05 M	0.05 g	0.4 g

Instruments: Infrared spectrum (KBr pellet) in the range of 4000 to 500 cm^{-1} was obtained using Fourier transform infrared spectrophotometer (FT-IR, Perkin-Elmer, 90,776) for structural identification of the synthesized composites. Powder XRD diffraction pattern was recorded at (Phillips X'pert Pro) with Cu*K*α radiation (0.154060 nm) by employing 45 kV voltage at X-ray diffraction scale 10º to 90º. Thermogravimetric analysis (TGA, Perkin Elmer-4000) were completed at temperature ran-ging from room temperature to 700 K in nitrogen atmosphere. The surface morphologies of the synthesized composites were examined through field-emission scanning electron micro-scope (FE-SEM, Carl Zeiss EVO40), energy dispersive X-ray spectroscopy (EDX,Carl Zeiss EVO40) and high resolution transmission electron microscopy (HR-TEM Technai, G2.30 STWIN). Cyclic voltammogram, galvanostatic charge/discharge and EIS (electrochemical impedance analysis) were performed through potentiostat dual channel/Autolab PGSTAT 86,472.

Electrochemical analysis: Electrochemical ability of the sample was calculated in 1M Na_2SO_4 electrolyte solution were examined at room temperature in three-electrode cell system in which the electroactive material was brush coated over grap-hite sheet with a area of 1 cm × 1 cm. The coated electrode was utilized as functioning electrode, platinum as a counter electrode and Ag/AgCl as a reference electrode. The functioning electrode was assembled by compressing a combination of synthesized electroactive material (70 wt%), acetylene black (20 wt%) and PVDF (10 wt%) as a binder of total electroactive mass. A slight

amount of DMF solvent was used to obtain homogenous slurry. Cyclic voltammograms were recorded at potential window -4 to 4 V (Ag/AgCl) at different sweep rate 5-100 mV/s. Whereas, in the galvanostatic charge/discharge (GCD) curves, which were calculated at various current densities of 3, 5, 5.5, 7 and 8 A/g (- 4 to 4V). ESI frequency range from 0.01 to 100,000 Hz was executed having an AC inflection of 5 mV in 1M Na_2SO_4 electrolyte solution.

RESULTS AND DISCUSSION

FTIR analysis: FTIR spectrum was recorded to characterize the molecular structure of SDS doped Pani-co/MWCNT (SD1), SDS doped Pani-co/CuO (SD2) and SDS doped Pani-co/MWCNT/CuO composite (SD3). As displayed in Fig. 1, all the composites exhibit the existence of quinoid band and benzenoid at 1480 and 1490 cm^{-1}, respectively. The characteristic wavenumber of Pani-co were observed at 1315 and 1172 cm^{-1} related to C-N stretching, -N-benzenoid-N- C=N stretching and -N=quinoid=N-, respectively [31]. The functional groups of C=O at 1650 cm^{-1} and C-O at 1380 cm^{-1} were characterized in CNT-COOH and these peaks were missing in SD2 sample, which confirmed the absence of MWCNT in SD2 nanocomposite [32]. The peak obtained at 1315 cm^{-1} can be assigned to C-N^{*+} stretching vibration in all the synthesized nanocomposites. The absorption band corresponding to metal-oxygen Cu-O stretching vibration in SD2 and SD3 was shifted to 595 cm^{-1} due to its interaction with MWCNT. The absorption peak at 756 to 665 cm^{-1} associated to the S-O and C-S stretching vibrations, and the peak at 835 cm^{-1} is related to the C-H out of plane bending vibration of 1,2,4-trisubstituted aromatic rings, which shows that -SO$_3$H group of SDS were attached directly on the aromatic rings [33-35].
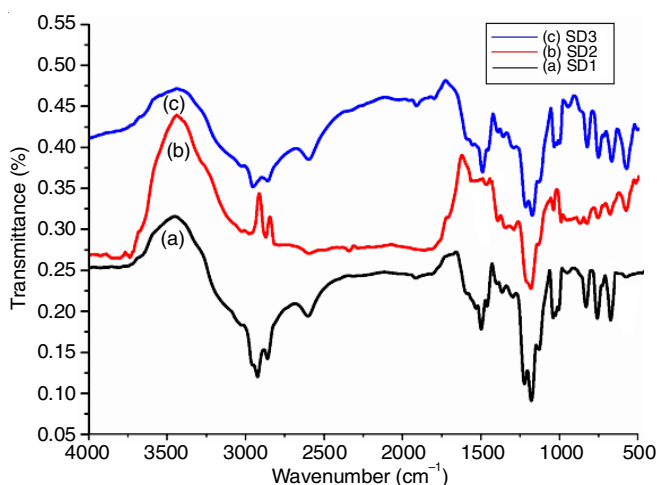

Fig. 1. FT-IR (AT) spectrum of: (a) SD1 (b) SD2(c) SD3 composites

XRD analysis: Fig. 2 illustrated the X-ray diffraction pattern of the synthesized composites SD1, SD2 and SD3. The characteristic diffraction peak (002) for MWCNT, were shifted to 19.5° due to its interaction with Pani-co. Peaks position at 15° (011) and 19.5° (200) are the reflection plane for Pani-co emeraldine salt, which indicates that Pani-co has its element structure in compounds composition [36,37]. The diffraction band corres-
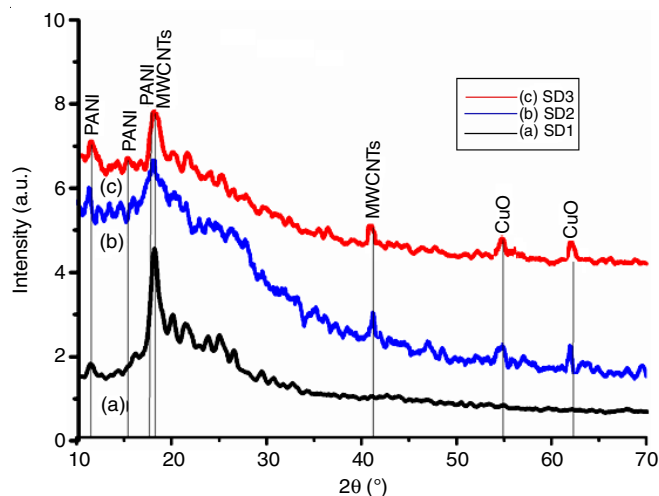

Fig. 2. X-ray diffraction graph of: (a) SD1 (b) SD2 (c) SD3 composites

ponding to 2θ values 43.3º, 55.4º and 63.1º related to plane (202), (020), (113) were assigned to face-cantered cubic CuO in agreement with the standard data of CuO (JCPDS card no. 89-2530) [38-40]. In all the synthesized samples, the peaks of metallic Cu and Cu_2O were not found indicating the purity of samples.

Thermal analysis: Thermogravimetric analysis has been utilized to examine the thermal stability of the composite with increasing thermal energy. In this method, change of mass has been calculated at different temperature and time under specific environment. Applying this tool, one can inspect the reaction kinetics of the procedure, thermal stability, degradation temperature, *etc*. Outcome of thermogravimetric studies for the synthesized nanocomposites are shown in Fig. 3. The results of thermogravimetric analysis shows three variant stages of reaction route which represents a removal of ingredient elements, moisture and water vapour, *etc*. and also indicate the polymeric chains degradation [41]. In the present inspection, first inflection of the all composite of thermal reactions happen approximately at 150 K, the second slope terminate around 400 K and the third slope hold on to the end *i.e.* approximate 700 K. Fascinatingly, in every slope the proportion of mass reduced with increasing amount of chemical addition. The inflections of MWCNTs happen between 500 and 700 ºC depending on the technique applied for the synthesis [42]. Decomposition of MWCNTs in SDS doped Pani-co/MWCNTs samples starts from 280 to 400 ºC. In the operating temperature range, Cu(OH)$_2$ possibly changes into CuO. One of the previous report [43] acknowledges the origin of CuO from Cu(OH)$_2$ element because of the progressive increase of temperature throughout thermal action. The working thermal treatment on the composite utilized to dehydrate Cu(OH)$_2$ into CuO and helps to achieve organized nanostructure. But this second slope of response too reduced in conditions of percentage of active mass converted as higher concentrations the CuO elements in the composite. The third slope indicates the inflection of polymeric chain [44]. The wet mass alter recorded in third slope of response is mostly because of the absolute inflection of quinoid rings. The degradation of build polymeric lattice structure also found to be reduced as in large amount of CuO. The influence of CuO in the Pani-co lattice have been explained above, which indicated that CuO
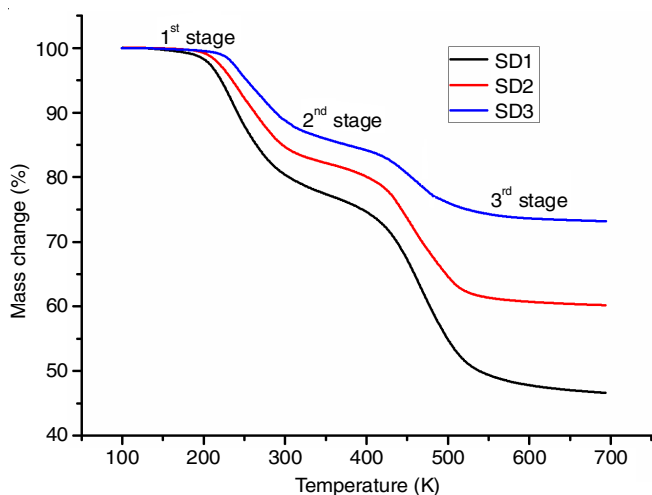
Fig. 3. TGA graph of SD1, SD2 and SD3 nanocomposite

helps the polymer to achieve organized crystalline structures and create dissimilar crystalline characteristics. The emergence of polycrystalline character in the polymeric nanocomposite is mostly credited to the role of CuO, which supports to achieve synchronized particle size organization. This arranged organization enhanced respectively with the increasing amount of CuO. It is the main reason for the decrease in the mass of the composite with high amount of CuO.

FESEM analysis: The FESEM micrographs of all the three composites are shown in Fig. 4. The FESEM micrographs were observed at high magnification. In SD1 sample (Fig. 4a), MW-CNTs was attached with the aromatic ring of SDS during p-p interactions; its dodecyl chain had maximum compatibility thus, SDS showed the dual nature in this system: acts as a surfactant and doping agent [45]. It provides more efficient dispersion of the MWCNTs without much coiling. The formation of SDS doped Pani-co was highly affected with the presence of CuO; the diameter and length of SDS doped Pani-co composite decreased dramatically. Fig. 4b showed that CuO was homogeneously dispersed in the polymer matrix. When CuO was fabricated in SDS solution, a thin SDS layer may form on their surface thus protecting it from oxidation by APS during polymerization [46]. Fig. 4c exhibits the FESEM micrograph of SDS doped Pani-co/CuO/MWCNTs nanocomposite, which noticeably illustrated the agglomerated coating of CuO nanoparticles along with SDS Pani-co and MWCNTs. The elemental composition analyses of SD1 sample (Fig. 4d) exhibited to the existence of C, O and N while sample SD3 and SD3 (Fig. 4e and F) displayed the existence of Cu, O, C and N.

HRTEM analysis: HR-TEM images of all the fabricated nanocomposites *viz*. SD1, SD2, and SD3 composites are displayed in Fig. 5. Due to functionalization of MWCNTs, it can easily adhere the SDS doped Pani on its surface which was clearly observed in sample SD1 (Fig. 5a). In Fig. 4b, sample SD2 clearly depicted the presence of CuO nanosphere of particle size of 9 to12 nm in an ultrafine layer of SDS doped Pani-co. Similar observation are seen in SD3 sample (Fig. 5c) where
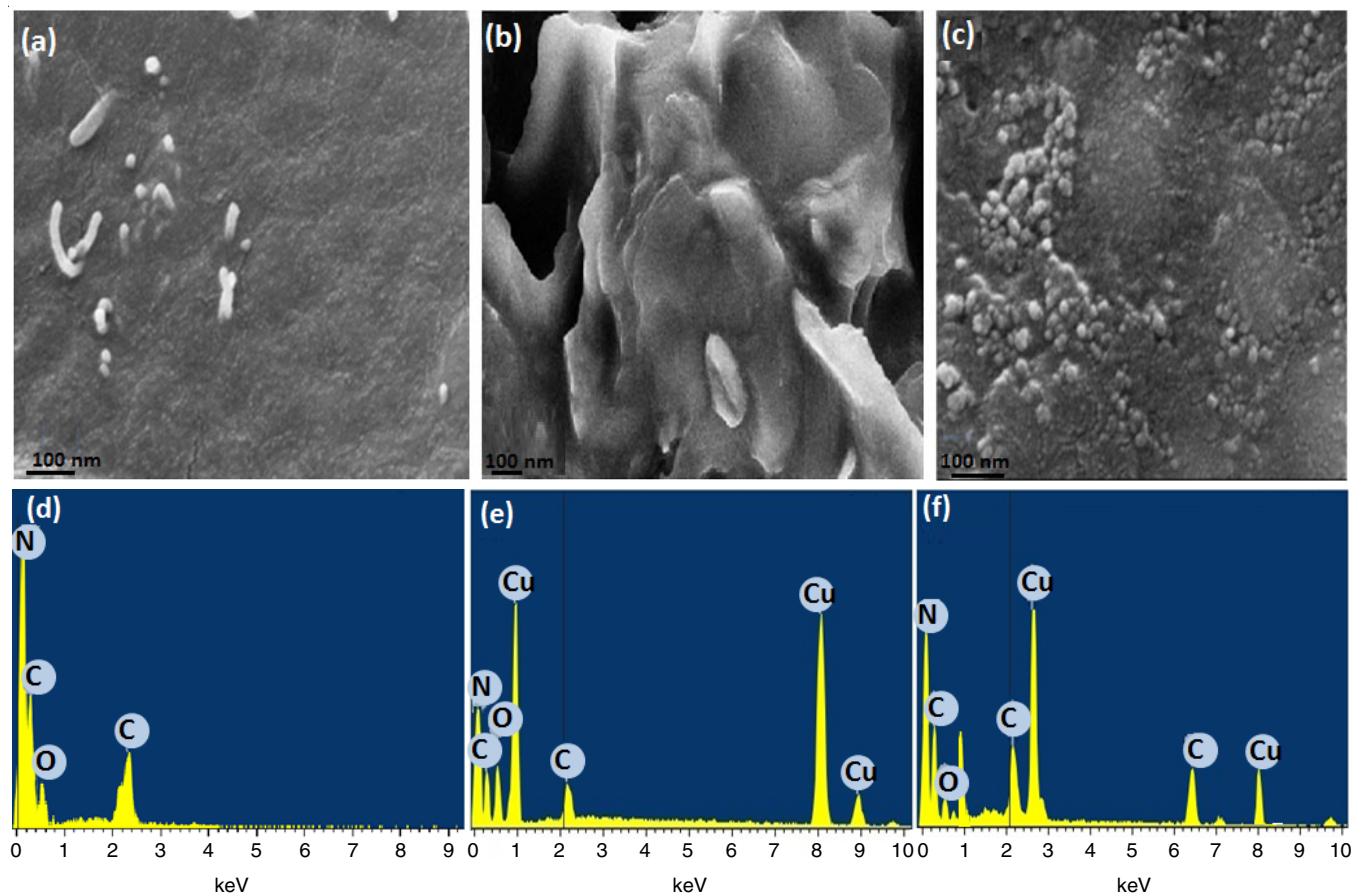

Fig. 4. FESEM image of (a) SD1 (b) SD2 (c) SD3; EDS spectra of (d) SD1 (e) SD2 (f) SD3 composites
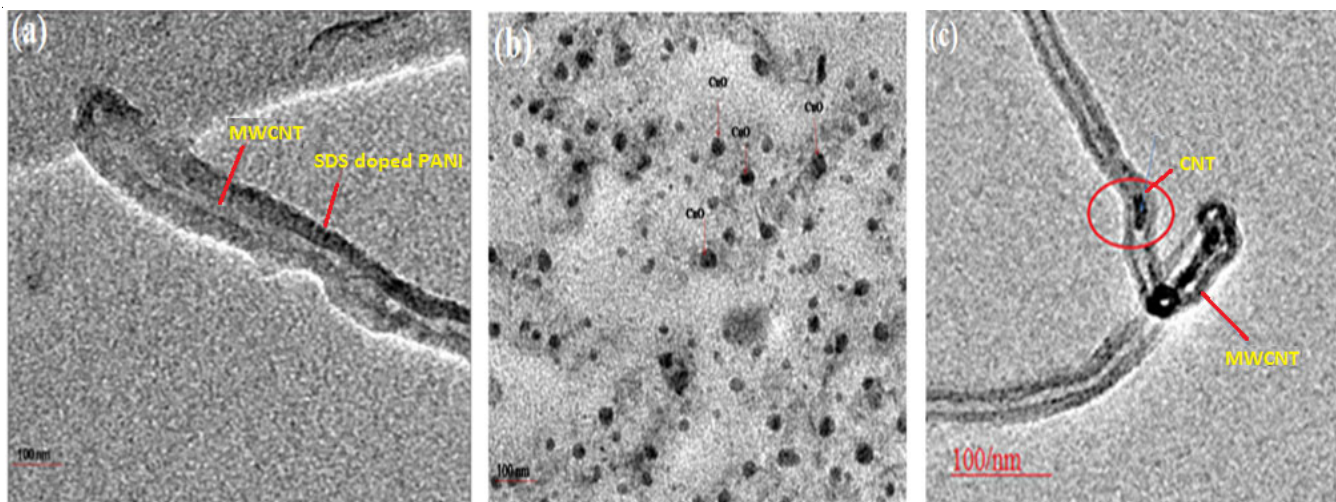
Fig. 5. HRTEM images of: (a) SD1 (b) SD2 (c) SD3 composites

very small CuO nanosphere were found to be encapsulated in the SDS doped Pani-co surface, which was further coated over MWCNTs [47-50].

Electrochemical characterization: Electrochemical property of the synthesized electroactive composites was investigated through cyclic voltammetry (CV) galvanostatic charge/discharge (GCD) and electrochemical impedance spectroscopic (EIS) study using three-electrode cell assembly from 5 mV/s to 50 mV/s at operating potential window (−0.4 to +0.4V) in 1M Na_2SO_4. Cyclic voltammetry of SDS doped Pani-co, SD1, SD2, also SD3, the electroactive composites cyclic voltammograms are display in Fig. 6a. These CV curves showed a rectangular shapes not involved in redox reaction, which indicate perfect pseudocapacitive characteristics. Furthermore, cyclic voltammograms still maintain comparatively rectangular curves without obvious variations when the sweep rate was improved from 5 to 50 mV/s as shown in Fig. 6b, signifies a rapid charge/discharge characteristics of the devices [51]. It is noticeably observed that composite SD3 depicted a higher current compared to other composite materials. The specific capacitances (C_{sp})

of the electroactive material were calculated by following eqn. 1 [52]:

$$C_{sp} = \int \frac{(I \times dV}{(\partial \times m \times \Delta V)} \tag{1}$$

where C_{sp} is the gravimetric capacitance/specific capacitance in F/g, m is the electroactive mass of material in the electrodes (g), I indicates gravimetric response current density A/g, consider as the average of anodic and cathodic peak current also ∂ represent sweep rate in mV/s, and m is the electroactive mass of composites in the electrodes (g). It is calculated by the following eqn 2:

$$M = \frac{(Q_{dep} \times MW_{mon})}{Z \times F} \tag{2}$$

In the above equation, Q_{dep} is deposited charge achieved by cyclic voltammetry technique. MW_{mon} is the molecular weight of monomer (g/mol).

Electroactive materials SD1, SD2 and SD3 displayed a specific capacitances of 487, 550 and 1485 F/g, respectively.
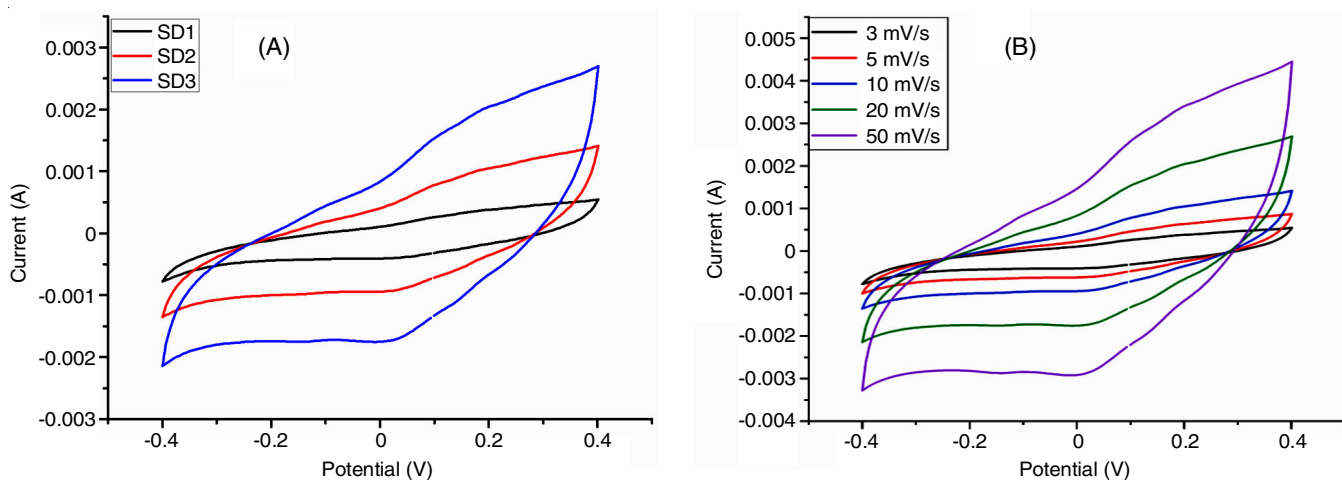

Fig. 6. (A) CV curve of SD1, SD2 and SD3 at 5mV/s in 1M Na_2SO_4 electrolyte solution and (B) CV curves of SD3 nanocomposite at different sweep rates (3mV/s, 5mV/s, 10mV/s, 20mV/s, and 50mV/s,) in 1M $Na_2SO_4.$
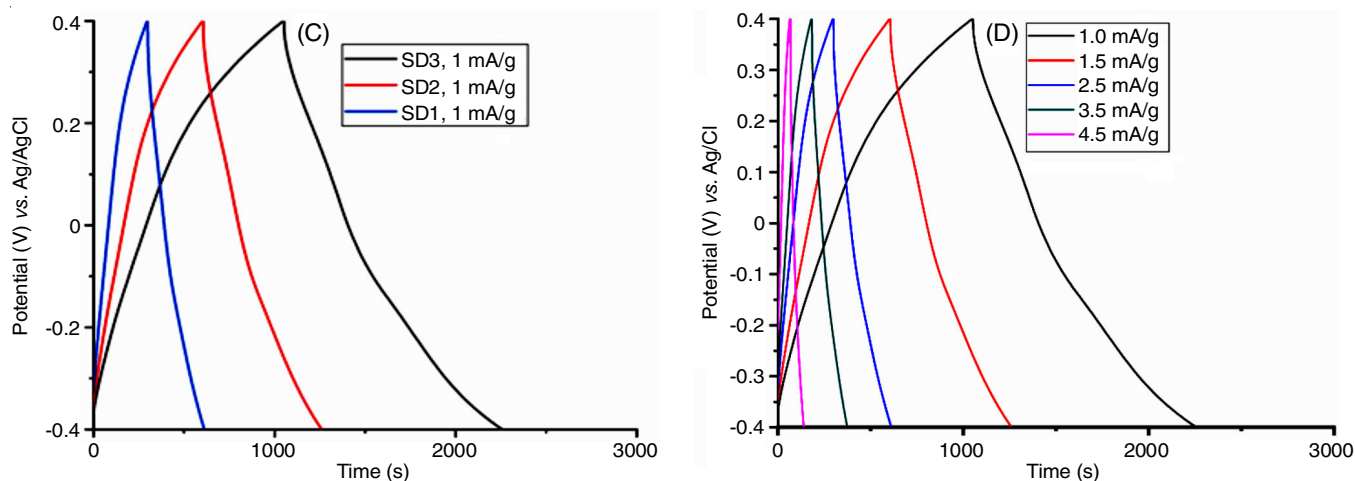
Fig. 7. (C) GCD curve of SD1, SD2 and SD3 at 1A/g in 1M Na_2SO_4 electrolyte solution (D) GCD curve of SD3 at various current density

Moreover, the specific capacitance of the electroactive material totally depends on the integrated CV curve area. As shown in Fig. 7a in case of SD1, that SDS doped Pani-co MWCNTs showed a minimum integrated area of curve, which enhances consistently in case of SD2 composite and further increased in SD3 composite. The development of the specific capacitance of the electroactive composites as related to the Pani-co is credited to the synergistic involvement of the three componets. In addition, MWCNTs can significantly control the morphology of the electroactive composites to present maximum surface area also it enhances the electrical conductance [53]. The MWCNTs CuO contributes the pseudo-capacitance with Faradic operation and SDS doped Pani also gives ELDC in the aqueous electrolyte/working electrode interactions. Furthermore, a layering at the MWCNTs/CuO of Pani-co prolonged the structure deterioration of Pani-co coating because shrinking/swelling procedure through ion insertion and de-insertion of the electrolyte [54]. Furthermore, the contribution of CuO activity shows an important character during the electrochemical performance, as it was noticed that SD3 shows maximum specific capacitance of 1485.7 F/g among the different electroactive materials reported in this work. An increase in capacitive value is noticed on extra doping of CuO in the composite denoted as SD3; indicating that the ratio of CuO present in composite SD3 are beneficial for that kind of ternary composites. Though, the capacitive nature can be credited to the morphological structure of the composite, although a comparatively well-organized and regular composition in SD3 is highly beneficial for rapid transportation of ions [55]. Sample SD3 was examined at various scanning rates as displayed in Fig. 7b. It is visibly observed that the anodic and cathodic peak current is enhanced by the enhancing the operating potential scan rates. To further investigate the electrochemical capacitance characteristics of the electroactive materials, a GCD (galvanostatic charge-discharge) experiment was executed in 1M Na_2SO_4. Fig. 7A exhibits the galvanostatic current charge-discharge curves of electroactive composite at 1 A/g, and the graph showed an irregular shape that indicate dual nature of the observed capacitance *i.e.* ELDC as well as pseudocapacitance characteristics. This can be credited

to the presence of various constituent materials in the synthesized nanocomposites. The CD areas (charging curves) are quite similar in their discharging pattern, an essential property of supercapacitors. SDS doped Pani-co indicates a maximum IR drop but after introducing MWCNTs/CuO in SD3 sample the IR drop reduction has been observed and displayed a low system resistance (electrode/electrolyte) present in the electroactive materials. The C_{sp} (specific capacitances) were obtained using the eqn. 3 [56]:

$$C_{sp} = \frac{i\Delta t}{m\Delta E} \qquad (3)$$

where C_{sp} is the gravimetric specific capacitance in (F/g); i is the gravimetric current density (A); Δt is the discharge time; m is the quantity weight loading of electroactive material in (g) and ΔE is the working potential window during charge/discharge. The highest linear potential-time profile was noticed for SD3 sample, which display the optimum capacitive performance. Determined the specific capacitances were 1512 F/g, 811F/g and 363 F/g at 1mA/g for SD1, SD2 and SD3 correspondingly as the current density increased, the specific capacitance enhanced by 75.9%. The effects of electrochemical GCD inspection were observed using the CD curves area. The synthesized nanocomposite SD3 was again inspected at different range of current densities of 1.0, 1.5, 2.5, 3.5 and 4.5 A/g and the calculated specific capacitance were 1512, 1230, 968, 861 and 360 F/g, respectively. The specific capacitance for SD3 sample was further improvised by 76.2% on increasing current density. The merged picture is displayed in Fig. 7d. It is observed that electrochemical charging-discharging curve perpetuate a equivalent structure at different current density, also the columbic efficiency is determined to be almost 90%, which deduce the enduring nature of the nanocomposite [57]. Stability as well as reversibility are the two significant characteristics of electroactive materials, which make its suitable utilization in energy storage devices.

The GCD cyclic consistency of electroactive material SD3 was explored at a current density of 3A/g. Fig. 8 displayed graph of composite SD3, which clearly indicated preservation
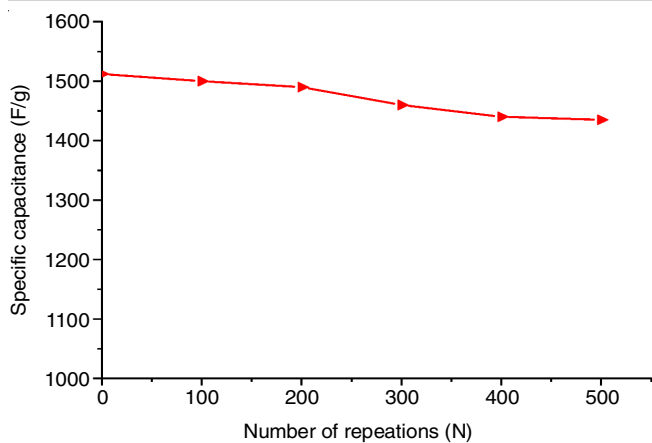
Fig. 8. Variation of the specific capacitance with various current densities for SD3 nanocomposite

of 90% in specific capacitance following 500 cycles. The result represents the durable cycle stability [58]. It was thus obtained due to the consistent coating of CuO over SDS doped Pani-co/MWCNTs surfaces, which enhanced the effective pseudo-capacitance and thus enhanced the cyclic life.

EIS was utilized to find out the ohmic resistance and charge transfer resistance characteristics of the electroactive material. In Fig. 9, the EIS value displayed the Nyquist plots between Img. Z″ capacitive line and Real Z′ Warburg diffusion line calculated from 1 mHz to100 kHz frequency region. The Re Z′-axis shows a approximate of the identical solution resistance or series resistance/source resistance (R_s) electroactive composites show a minute Real (Z′) axis intercept and a pinpoint semicircle while SD3 showed a minimal semicircle at higher frequency and propounds a minimum internal ohmic resistance of electro-active materials [59]. The accurate corresponding electrical network circuit was designed for the SD1, SD2 and SD3 electro-active materials. The source resistance (R_s) acquired for electro-active composites SD3 were 1.23 Ω. This reduced ohmic value of source resistance (R_s) in the synthesized composites notifies the better conductivity of the electroactive composites compared with SD1 and SD2 composites [60]. The minimal value of source resistance (R_s) was noticed in SD3 composite with the distinct electroactive composites, which are also in agreement with the
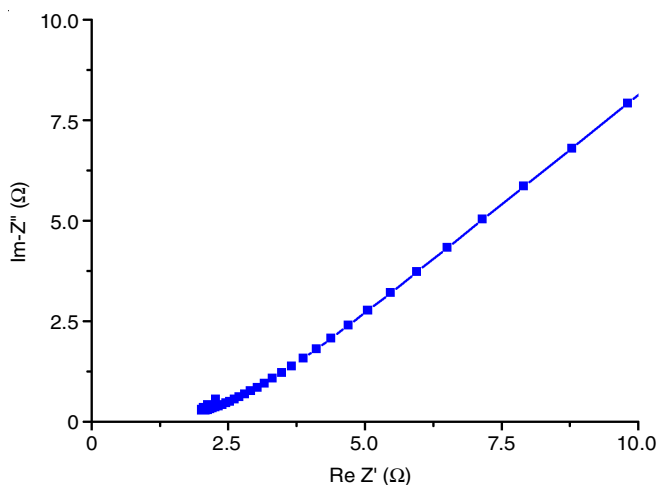
CV and GCD results [61]. Furthermore, at the minimal frequency range, the perpendicular slope parallel to the Im-Z″ axis showed an idealistic capacitive nature of the electroactive composite, which illustrated that the cell originally functions in the diffusion relatively than absorption controlled system [62].

The energy density (E) and power density (P) evaluated through the constant current GCD cycle form the following equations [63]:

$$E = \frac{C_s \Delta U2}{2} \tag{4}$$

$$P = \frac{E}{\Delta t} \tag{5}$$

where C_s indicate the specific capacitance of a capacitor obtain through eqn. 1; Δt and Δu are the discharge time and potential window from the end of charge/discharge, respectively [64]. The actual capacitance from the impaired semicircle form (for example a constant phase element similar along to the resistor) can be obtained from eqn. 6:

$$C = \frac{(Q \times R)^{1/4}}{R} \tag{6}$$

From eqn. 6, the capacitances of SDS doped Pani-co/MWC-NTs/CuO electrode calculated in 1M Na_2SO_4 were around equal to 0.079 cm^{-2} [65]. The capacitive values of capacitance accor-ding to the EIS examination are excellent agreement through experimental value achieved by the CV and GCD curves.

Conclusion

A novel electroactive composite of SDS doped poly-(aniline-2-isopropylaniline) MWCNTs/CuO nanocomposite have been successfully synthesized *via in situ* oxidative chemical polymerization procedure. Incorporation of MWCNTs and CuO was found to improve both the crystalline nature and the electroactivity as well. The electroactive nanocomposite exhi-bited high thermal stability. Cyclic voltammgram of a thin coating of electroactive composite SD3, display maximum capacitance of 1485.7 F/g at sweep rate of 5 mV/s. Thus, this composite could be used as an encouraging electroactive composite elect-rode material for super-capacitor applications.

REFERENCES

1. G. Chitra and T.C. Thanu, *J. Inorg. Organomet. Polym.*, **27**, 1491 (2017); https://doi.org/10.1007/s10904-017-0608-7
2. D. Zare-Hosseinabadi, A. Ershad-Langroudi and A. Rahimi, *J. Inorg. Organomet. Polym..*, **20**, 250 (2010); https://doi.org/10.1007/s10904-010-9334-0
3. Y. Ghandour, I. Mestiri and M.S. Belkhiria, *J. Inorg. Organomet. Polym.*, **27**, 685 (2017); https://doi.org/10.1007/s10904-017-0511-2
4. S. Verma, S.S. Amritphale, S.K. Sanghi and S. Das, *J. Inorg. Organomet. Polym.*, **27**, 728 (2017); https://doi.org/10.1007/s10904-017-0517-9

Fig. 9. Nyquist plot of SD3 nanocomposite

5. M. Yousefi and M. Ranjbar, *J. Inorg. Organomet. Polym.*, **27**, 633 (2017);
    https://doi.org/10.1007/s10904-017-0504-1

6. A.G. Macdiarmid, S.L.Mu, N.L.D. Somasiri and W. Wu, *Mol.Cryst. Liq. Cryst.*, **121**, 187 (1985);
    https://doi.org/10.1080/00268948508074859

7. E.W. Paul, A.J. Ricco and M.S. Wrighton, *J. Phys. Chem.*, **89**, 1441 (1985);
    https://doi.org/10.1021/j100254a028

8. O.P.H. Vaughan, G. Kyriakou, N. Macleod, M. Tikhov and R.M. Lambert, *J. Catal.*, **236**, 401 (2005);
    https://doi.org/10.1016/j.jcat.2005.10.019

9. I.S. Park, M.S. Kwon, Y. Kim, J.S. Lee and J. Park, *Org. Lett.*, **10**, 497 (2008);
    https://doi.org/10.1021/ol702790w

10. D. Prakashbabu, H.B. Ramalingam, R. Hari Krishna, B.M. Nagabhushana, R. Chandramohan, C. Shivakumara, J. Thirumalai and T. Thomas, *Phys. Chem. Chem. Phys.*, **18**, 29447 (2016);
    https://doi.org/10.1039/c6cp04633a

11. M.E. Jozefowicz, A.J. Epstein, J.P. Pouget, J.G. Masters, A. Ray and A.G. MacDiarmid *Macromolecules*, **24**, 5863 (1991);
    https://doi.org/10.1021/ma00021a022

12. L.I. Nadaf and K.S. Venkatesh, *Mater. Sci. Res.*, **12**, 108 (2015);
    https://doi.org/10.13005/msri/120204

13. P.S. Vijayanand, J. Vivekanandan, A. Mahudeswaran, G. Ravi Kumar and R. Anandarasu, *Design Monom. Polym.*, **18**, 12 (2015);
    https://doi.org/10.1007/s13726-013-0191-x

14. Y. Wang, J. Guo, T. Wang, J. Shao, D. Wang and Y.-W. Yang, *Nanomaterials*, **5**, 1667 (2015);
    https://doi.org/10.3390/nano5041667

15. A. Becerra, S. Rodriguez-Llamazares, C. Carrasco, J. Diaz-Visurraga, C. Riffo and M.A. Mondaca, *High Perform. Polym.*, **25**, 51 (2012);
    http://doi.org/10.1177/0954008312454899

16. K. Siddique, B.K. Nath and S. Karmakar, *Int. J. Nanosci.*, **12**, 1350036 (2013);
    https://doi.org/10.1142/S0219581X13500361

17. Y. Xiong, I. Washio, J. Chen, H. Cai, Z. Li and Y. Xia, *Langmuir*, **22**, 8563 (2006);
    https://doi.org/10.1021/la061323x

18. R. Amrani, F. Pichot, L. Chahed and Y. Cuminal, *Cryst. Struct. Theory Appl.*, **1**, 62 (2012);
    http://doi.org/10.4236/csta.2012.13012

19. Y. Peng, Z. Liu and Z. Yang, *Chin. J. Chem.*, **27**, 1086 (2009);
    http://doi.org/10.1002/cjoc.200990181

20. H.S.O. Chan, S.C. Ng, W.S. Sim, K.L. Tan and B.T.G. Tan, *Macromolecules*, **26**, 144 (1993);
    https://doi.org/10.1021/ma00053a022

21. L. Jin, X. Zhao, X. Qian and M. Dong, *J. Colloid Interface Sci.*, **509**, 245 (2018);
    https://doi.org/10.1016/j.jcis.2017.09.002

22. K. Weiser, *Progr. Solid State Chem.*, **11**, 403 (1976);
    https://doi.org/10.1016/0079-6786(76)90002-9

23. H. Wang, J.Z. Xu, J.J. Zhu and H.Y. Chen, *J. Cryst. Growth*, **244**, 84 (2002);
    https://doi.org/10.1016/j.jtusci.2014.04.006

24. J. Davenas, M. Chouiki, S. Besbes, A. Ltaief, H. ben Ouada, A. Bouazizi, H. Trad and M. Majdoub, *Synsth. Met.*, **139**, 617 (2003);
    https://doi.org/10.1016/ S0379-6779(03)00266-2

25. R. Jacob, A.P. Jacob and D.E. Mainwaring, *J. Mol. Struct.*, **933**, 77 (2009);
    https://doi.org/10.1016/j.molstruc.2007.05.041

26. K. Tian, C. Liu, H. Yang and X. Ren, *Colloids Surf.*, **397**, 12 (2012);
    https://doi.org/10.1016/j.colsurfa.2012.01.019

27. K.M. Ziadan, H.F. Hussein and K.I. Ajeel, *Energy Proc.*, **18**, 157 (2012);
    https://doi.org/10.1016/j.egypro.2012.05.027

28. T.M.D. Dang, T.T.T. Le, E. Fribourg-Blanc and M.C. Dang, *Adv. Nat. Sci.: Nanosci. Nanotechnol.*, **2**, 015009 (2011);
    http://dx.doi.org 10.1088/2043-6262/2/1/015009

29. R.V. Kumar, Y. Mastai, Y. Diamant and A. Gedanken, *J. Mater. Chem.*, **11**, 1209 (2001);
    https://doi.org/10.1039/b005769j

30. L.Q. Pham, J.H. Sohn, C.W. Kim, J.H. Park, H.S. Kang, B.C.Lee and Y.S. Kang, *J. Colloid Interface Sci.*, **365**, 103 (2012);
    https://doi.org/10.1016/j.jcis.2011.09.041

31. Y.W. Lin, H.H. Chang, Y.S. Liu, M.C. Tsai, Y.C. Tsai and T.M. Wu, *J. Electrochem. Soc.*, **157**, K15 (2010);
    http://doi.org/10.1149/1.3254159

32. S. Bilal, S. Farooq, A. Shah and R. Holze, *Synth. Met.*, **197**, 144 (2014);
    https://doi.org/10.1016/j.synthmet.2014.09.003

33. X.Z. Wang, C.L. Ho, L. Yan, X. Chen, X. Chen, K.-Y. Cheung and W.-Y. Wong, *J. Inorg. Org. Polym. Mater.*, **20**, 478 (2010);
    https://doi.org/10.1007/s10904-010-9371-8

34. W. Ho, J.C. Yu and S. Lee, *Chem. Commun.*, 1115 (2006);
    https://doi.org/10.1039/B515513D

35. A.K. Sharma, P. Bhardwaj, S.K. Dhawan and Y. Sharma, *Adv. Mater. Lett.*, **6**, 414 (2015);
    https://doi.org/10.5185/amlett.2015.5690

36. G. Chaudhary, A.K. Sharma, P. Bhardwaj, K. Kant, I. Kaushal and A.K. Mishra, *J. Energy Chem.*, **26**, 175 (2017);
    https://doi.org/10.1016/j.jechem.2016.09.013

37. G. Chaudhary, A.K. Sharma, I. Kaushal and P. Saharan, *Asian J. Chem.*, **30**, 2158 (2018);
    https://doi.org/10.14233/ajchem.2018.21500

38. H. Yan and K. Kou, *J. Mater. Sci.*, **49**, 1222 (2014);
    https://doi.org/10.1007/s10853-013-7804-9

39. R. Singhal and V. Kalra, *J. Mater. Chem. A*, **3**, 377 (2015);
    https://doi.org/10.1039/C4TA05121A

40. D. Prakashbabu, H.B. Ramalingam, R.H. Krishna, B.M. Nagabhushana, R.Chandramohan, C. Shivakumara, J. Thirumalai and T. Thomas, *Phys. Chem. Phys.*, **29447**, 29457 (2016);
    https://dx.doi.org/10.1039/C6CP04633A

41. J. Agrisuelas, C. Gabrielli, J.J. García-Jareno, H. Perrot and F. Vicentec, *Electrochim. Acta*, **561**, 573 (2014);
    https://doi.org/10.1016/j.electacta.2014.04.047

42. L.I. Nadaf and K.S. Venkatesh, *Mater. Sci. Res.*, **108**, 111 (2015);
    https://doi.org/10.13005/msri/120204

43. M.A.A.M. Abdah, N.S.M. Razali, P.T. Lim, S. Kulandaivalu and Y. Sulaiman, *Mater. Chem. Phys.*, **120**, 128 (2018);
    https://doi.org/10.1016/j.matchemphys.2018.08.018

44. O. Alekseeva, S. Chulovskaya, N. Bagrovskaya and V. Parfenyuk, *Chem. Chem. Technol.*, **447**, 450 (2011);
    https://doi.org/10.23939/chcht05.04.447

45. L.S. Ghadimi, N. Arsalani, A.G. Tabrizi, A. Mohammadi and I. Ahadzadeh, *Electrochim. Acta*, **116**, 127 (2018);
    https://doi.org/10.1016/j.electacta.2018.05.160

46. A.D. Manasrah, I.W. Almanassra, N.N. Marei, U.A. Al-Mubaiyedh, T. Laoui and M.A. Atieh, *RSC Adv.*, **8**, 1791 (2018);
    https://doi.org/10.1039/c7ra10406e

47. U.S. Belgamwar and N.N. Sharma, *AIP Conf. Proc.*, **1724**, 020065 (2016);
    https://doi.org/10.1063/1.4945185

48. P.K. Tyagi, I. Janowska, O. Cretu, C. Pham-Huu and F. Banhart, *J. Nanosci. Nanotechnol.*, **11**, (2011);
    https://doi.org/10.1166/jnn.2011.3740

49. Z. Abdi and S. Sedaghat, *Int. J. Nano Dimen.*, **25**, 32, (2016);
    https://doi.org/10.7508/ijnd.2016.01.003

50. Y. Peng and Q. Chen, *Nanotechnology*, **20**, 235606 (2009);
    https://doi.org/10.1088/0957-4484/20/23/235606

51. M.S.S. Dorraji, I. Ahadzadeh and M.H. Rasoulifard, *Int. J. Hydrogen Energy*, **39**, 9350 (2014);
    https://doi.org/10.1016/j.ijhydene.2014.03.242
    https://doi.org/10.1016/j.ijhydene.2014.03.242

52. J. Tian, C. Cui, C. Zheng and W. Qian, *Chin. Chem. Lett.*, **599**, 602 (2018);
    https://doi.org/10.1016/j.cclet.2018.01.027

53. R. Zhang, Y. Liao, S. Ye, Z. Zhu and J. Qian, *R. Soc. Open Sci.*, **171**, 365 (2017);
    https://doi.org/10.1098/rsos.171365

54. R. Yuksel, C. Durucan and H.E. Unalan, *J. Alloys Comp.*, **658**, 183 (2016);
    https://doi.org/10.1016/j.jallcom.2015.10.216

55. V.V. Abalyaeva, G.V. Nikolaeva and O. N. Efimov, *Russ. J. Electrochem.*, **44**, 828 (2008);
    https://doi.org/10.1134/S1023193508070094

56. L.Y. Meng and S.J. Park, *Carbon Lett.*, **89**, 104 (2014);
    https://doi.org/10.5714/CL.2014.15.2.089

57. I. Kovalenko, D.G. Bucknall and G. Yushin, *Adv. Funct. Mater.*, **20**, 3979 (2010);
https://doi.org/10.1002/adfm.201000906

58. M.H. Al-Saleh and U. Sundararaj, *Carbon*, **47**, 2 (2009);
https://doi.org/10.1016/j.carbon.2008.09.039

59. L. Feng, N. Xie and J. Zhong, *Materials*, **7**, 3919 (2014);
https://doi.org/10.3390/ma7053919

60. A.M. Cojocariu, M. Soroceanu, L. Hrib, V. Nica and O.F. Caltun, *Mater. Chem. Phys.*, **135**, 728 (2012);
https://doi.org/10.1016/j.matchemphys.2012.05.051

61. A.L.M. Reddy, M.M. Shaijumon, S.R. Gowda and P.M. Ajayan, *J. Phys. Chem. C*, **114**, 668 (2010);
https://doi.org/10.1021/jp908739q

62. E.M. Genies and M. Lapkowski, *J. Electroanal. Chem. Interf. Electrochem.*, **220**, 67 (1987);
https://doi.org/10.1016/0022-0728(87)88005-1

63. Y.K. Zhou, B.L. He, W.J. Zhou, J. Huang, X.H. Li, B. Wu and H.L. Li, *Electrochim. Acta*, **49**,257(2004);
https://doi.org/10.1016/j.electacta.2003.08.007

64. S.K. Chang, K.T. Lee, Z. Zainal, K.B. Tan, N.A. Yusof, W.M.D.W. Yusoff, J.F. Lee and N.L. Wu, *Electrochim. Acta*, **67**, 67 (2012);
https://doi.org/10.1016/j.electacta.2012.02.014

65. P. Xiong, C. Hu, Y. Fan, W. Zhang, J. Zhu and X. Wang, *J. Power Source*, **266**, 384 (2014);
https://doi.org/10.1016/j.jpowsour.2014.05.048